Energy Advances

ROYAL SOCIETY OF CHEMISTRY

PAPER

View Article Online
View Journal | View Issue

Check for updates

Cite this: *Energy Adv.*, 2022, 1, 269

Lithium ion transport in solid polymer electrolyte filled with alumina nanoparticles†

Jiaqi Wang, Linhao Fan, Qing Du* and Kui Jiao *

Received 25th January 2022,
Accepted 14th March 2022

DOI: 10.1039/d2ya00025c

rsc.li/energy-advances

Using a solid polymer electrolyte (SPE) is a promising approach for improving lithium battery durability by suppressing the growth of lithium dendrites. However, the low conductivity at room temperature significantly limits its commercial application. In this work, Al_2O_3 nanoparticles are used as a filler in a SPE with polyethylene oxide (PEO) and lithium bis(trifluoromethanesulfonyl)imide (LiTFSI) salt to improve its conductivity, and the resulting structure and transport properties are analyzed in detail using molecular dynamics simulations. The results show that the addition of Al_2O_3 nanoparticles decreases the crystallinity and increases the degree of order of the PEO chains and makes it easier for Li^+ to combine with the PEO chains, thereby significantly enhancing Li^+ transport along the PEO chains. Moreover, the addition of Al_2O_3 provides an additional Li^+ transport path, which is the interface between the Al_2O_3 and PEO chains. Therefore, after adding Al_2O_3 nanoparticles, the conductivity is increased by 192.25% and 248.94% at 333 and 300 K, respectively, for the SPE with shorter PEO chains and by 225.2% and 285% at 333 and 300 K, respectively, for the SPE with longer PEO chains. Moreover, the enhancement effects of Al_2O_3 nanoparticles on conductivity are more significant for SPEs with longer PEO chains at lower temperatures.

Open Access Article. Published on 15 March 2022. Downloaded on 2/16/2026 9:13:57 PM.
This article is licensed under a Creative Commons Attribution 3.0 Unported Licence.

1. Introduction

Environmental pollution and global energy consumption have led to electric vehicles emerging as the main mode of future transportation.[1,2] Lithium batteries are the main candidates for electric vehicles and hybrid vehicles, and the usage of lithium metal as the anode provides the highest theoretical energy density for secondary lithium batteries.[3] However, lithium metal anodes and liquid electrolytes can easily generate lithium dendrites during charge and discharge processes, which cause internal short circuits in the lithium battery.[4] Meanwhile, liquid electrolytes have many disadvantages, such as easy leakage of the liquid and flammable reaction products.[5,6] In contrast, solid-state batteries using solid polymer electrolytes (SPEs) have the advantages of high ionic conductivity, high specific energy, solvent-free conditions, a wide electrochemical stability window, light weight, and easy processing.[7] As an SPE, polyethylene oxide (PEO) membranes doped with lithium salts have attracted great attention in recent years.[8–10] The PEO-based film is a flexible solid electrolyte with a low glass transition temperature (T_g), high dielectric constant, and certain mechanical strength, which can be used for special electronic devices.[11,12]

The conductivity in the PEO-based SPE greatly depends on the dynamic properties of the PEO chains. The properties of PEO-based structures depend strongly on the chain length. Shorter chains tend to be more flexible and enable larger ionic diffusion coefficients, while longer chains have higher mechanical stability.[13] The PEO chain contains ether coordination sites and can dissociate lithium salts.[14] Traditional lithium salts have been found to accumulate in SPEs. With increasing salt concentration and temperature, the degree of anion aggregation increases, which is related to the size of the anions.[15] Lithium bis(trifluoromethanesulfonyl)imide (LiTFSI) is a lithium salt with high chemical stability that is commonly used in SPE. Many studies have found that LiTFSI is largely dissociated in PEO matrices.[16] PEO has a flexible macromolecular chain, which benefits Li^+ transport.[17] Several Li^+ transport pathways have been observed in simulation studies, such as Li^+ moving along the PEO chains, Li^+ complexing and decomplexing with anions, and Li^+ occasionally hopping between the adjacent PEO chains.[18–20] Borodin *et al.*[15] showed that Li cations moving along the PEO chains generally show stronger mobility than those that jump between the PEO chains, suggesting that enhancing the movement along the PEO chains can significantly promote Li^+ diffusion.

However, the low conductivity of PEO/LiTFSI electrolytes at room temperature limits their application.[21] Generally, adding nanoparticle fillers is the best way to improve the conductivity

State Key Laboratory of Engines, Tianjin University, 135 Yaguan Road, Tianjin 300350, China. E-mail: duqing@tju.edu.cn, kjiao@tju.edu.cn

† Electronic supplementary information (ESI) available: Additional analysis and data (the mean square displacement in different systems, the diffusivities in the LC system, and the coordination number in different systems) are provided in the supplementary material. See DOI: 10.1039/d2ya00025c

© 2022 The Author(s). Published by the Royal Society of Chemistry

Open Access Article. Published on 15 March 2022. Downloaded on 2/16/2026 9:13:57 PM.
This article is licensed under a Creative Commons Attribution 3.0 Unported Licence.

by decreasing the crystallinity of the PEO chains and increasing the conductive area of Li^+. Moreover, the addition of nanoparticles can improve the interface stability and the mechanical strength of the SPEs.[22] According to previous studies, nanoparticle fillers for SPEs include passive fillers such as SiO_2,[23,24] Al_2O_3,[25,26] ZnO,[27] and $BaTiO_3$[28] and active fillers such as LLZO ($Li_7La_3Zr_2O_{12}$).[29] It is difficult for active fillers to tune surface interaction against the polymer matrix and the synthesis process is complex. However, the passive fillers are tunable, easily prepared, and inexpensive.[30] B. Scrosati and his collaborators[31] used TiO_2 functionalized with silane organic groups to improve the PEO electrolyte properties, which improved the conductivity. The nanoparticles interact with the PEO chains, resulting in a decrease in the crystallinity of the PEO chains. And Al_2O_3 as a high-stability and easily prepared passive filler can improve the conductivity and the mechanical strength of the SPEs.[32]

Molecular dynamics (MD) simulation is a powerful tool that can obtain insights into transport phenomena at the molecular level.[33] V. Ponce *et al.*[34] theoretically analyzed the charging process of a nanobattery with $LiCoO_2$ as the cathode, $Li_7P_2S_8I$ as the solid electrolyte, and lithium metal as the anode by MD simulations. J. Brooks and coworkers[13] investigated the structure and diffusion properties of PEO/LiTFSI electrolytes, indicating that Li cations mostly diffuse along the polymer chains instead of jumping between different polymer chains. Li *et al.*[35] elucidated the effects of the size and shape of nanoparticles on the ionic conductivity of PEO/$LiClO_4$ electrolyte through MD simulations, but the concentrations of nanoparticles were ignored. However, to the best of our knowledge, studies on the effect mechanism of nanoparticle fillers on the conductivity of SPEs are absent. In this work, MD simulations are carried out to investigate the conductivity of PEO/LiTFSI electrolytes filled with Al_2O_3 nanoparticles. The structures of the solid-state battery and SPE filled with Al_2O_3 are shown in Fig. 1. Meanwhile, the effects of PEO chain length and temperature are also studied.

2. Models and methods

2.1. Molecular models

A periodic boundary condition is applied in all three dimensions. The bulk electrolyte is based on PEO chains and LiTFSI salt. In this work, the interatomic interactions are described by the OPLS all-atom (OPLSAA) force field, which was developed for polymers and organic materials.[36] The potential energy for PEO molecules, Li^+, $TFSI^-$, and Al_2O_3 nanoparticles is expressed as:

$$u_{\text{bonds}} = \sum_{\text{bonds}} k_l(l - l_0)^2 \quad (1)$$

$$u_{\text{angles}} = \sum_{\text{angles}} k_\theta(\theta - \theta_0)^2 \quad (2)$$

$$u_{\text{dihedrals}} = \frac{1}{2}\sum_{\text{torsions}} V_{t,1}(1 + \cos(\omega + \delta_1)) + V_{t,2}(1 - \cos(2\omega + \delta_2)) + V_{t,3}(1 + \cos(3\omega + \delta_3)) \quad (3)$$

$$u_{\text{nb}} = \sum_{i<j}\left(\frac{Cq_iq_j}{r_{ij}}\right) + 4\varepsilon_{ij}\left(\frac{\sigma_{ij}^{12}}{r_{ij}^{12}} - \frac{\sigma_{ij}^{6}}{r_{ij}^{6}}\right) \quad (4)$$

where eqn (1), (2), and (3) are used to compute the interactions of bond stretching, bond angle bending, and dihedral torsion, respectively, and eqn (4) is used to compute the nonbonding interactions, *i.e.*, the van der Waals interactions and the electrostatic interactions by the Lennard-Jones (L-J) potential model and the long-range Coulomb potential model, respectively. Moreover, the Lorentz–Berthelot mixing rule is used to obtain the L-J interaction parameters between different types of atoms:

$$\varepsilon_{ij} = \sqrt{\varepsilon_{ii}\varepsilon_{jj}} \quad (5)$$

$$\sigma_{ij} = \frac{1}{2}(\sigma_{ii} + \sigma_{jj}) \quad (6)$$

The cutoff distance of the L-J potential is set as 1 nm. Furthermore, the particle–particle particle-mesh (pppm) solver with an accuracy of 0.0001 is used to calculate the long-range electrostatic interactions. The Nose–Hoover thermostat is used to control the system temperature with a relaxation time of 0.1 ps. The LAMMPS package is used for all MD simulations.[37]

To study the effects of Al_2O_3 nanoparticles on the properties of SPEs with different chain lengths, two types of PEO chains with different lengths are constructed in this work, a short-chain PEO molecular (SC) system and a long-chain PEO molecular (LC) system, as listed in Table 1. The SC system is composed of 40 Li cations, 40 TFSI anions, and 40 PEO chains including methyl end groups as well as 20 EO units, while the LC system is composed of 100 Li cations, 100 TFSI anions, and 20 PEO chains including methyl end groups as well as 100 EO units, which are commonly used to study the performance of SPEs.[33,35,38] The PEO chains

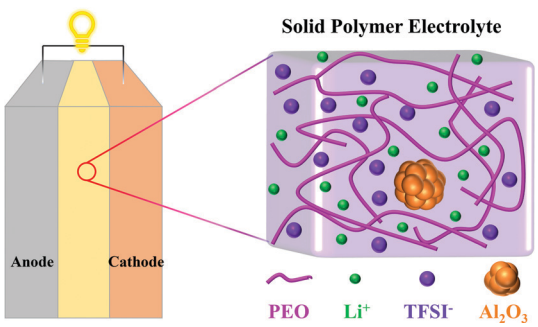

Fig. 1 Structures of the solid-state battery and SPE filled with Al_2O_3.

Table 1 Parameters of different systems ([EO]/chain is the number of EO units in each PEO chain, N_{chain} is the number of PEO chains in the system, N_{LiTFSI} is the number of LiTFSI in the system, and EO:Li is the number ratio of EO chains and Li cations)

System	[EO]/chain	N_{chain}	Mw (g mol^{-1})	N_{LiTFSI}	EO : Li
SC, 300 K	20	40	926	40	20 : 1
SC, 333 K	20	40	926	40	20 : 1
LC, 300 K	100	20	4446	100	20 : 1
LC, 333 K	100	20	4446	100	20 : 1

© 2022 The Author(s). Published by the Royal Society of Chemistry

Open Access Article. Published on 15 March 2022. Downloaded on 2/16/2026 9:13:57 PM.
This article is licensed under a Creative Commons Attribution 3.0 Unported Licence.

including methyl end groups have better ionic conductivity.[14] Plasticizers are absent in this work, considering that the main function of plasticizers is to reduce the crystallinity of PEO chains and their exclusion will not affect the conclusions of this work.

2.2. Alumina structure

The crystal structure of Al_2O_3 nanoparticles is a trigonal crystal system. In the simulation system, the Al_2O_3 nanoparticle contains 30 atoms, including 12 Al atoms and 18 O atoms (a = 5.178 Å^{-1}, b = 5.178 Å^{-1}, c = 5.178 Å^{-1}, α = 55.290°, β = 55.290°, γ = 55.290°).[39] Since this study mainly explores the effect of the concentration of nanoparticles on the SPE, the size and shape of the nanoparticles are fixed, and the interaction within the nanoparticles is ignored in the simulation process. The size of the Al_2O_3 nanoparticles is approximately 1.3 nm, which was selected because smaller nanoparticles are known to have a better enhancement effect.

The L-J potential parameters for O and Al atoms in the Al_2O_3 nanoparticles are σ_0 = 0.28 nm, ε_0 = 0.155 kcal mol^{-1} and σ_{Al} = 0.22 nm, ε_{Al} = 0.155 kcal mol^{-1}, respectively, while the atomic charges of O and Al atoms are −0.9450 e and +1.4175 e,[40] respectively. For the same temperature and PEO chain length, the concentrations of Al_2O_3 are determined by the number of Al_2O_3 nanoparticles, meaning that the concentrations of Al_2O_3 are a little different in different systems. Previous experiments showed that the addition of nanoparticles also has an important effect on the electrode–electrolyte interface, wherein the nanoparticles stabilize the electrode–electrolyte interface and reduce the interface impedance.[41,42] However, the electrode–electrolyte interface is not studied in this paper. More MD simulations will be carried out to study the effect of Al_2O_3 nanoparticles on the properties of the electrode–electrolyte interface in the future.

2.3. Simulation procedures

The initial temperature of all simulations is 300 K, while the initial pressure of all simulations is 100 atm using a timestep of 1 fs. The temperature was raised to 500 K, and the pressure was dropped to 1 atm during a 1 ns *NPT* (constant number of atoms, constant pressure, and constant temperature) simulation. Then, the systems were run at 500 K for 2 ns under an *NVT* (constant number of atoms, constant volume, and constant temperature) ensemble. The system temperature is varied between 300 K and 500 K four times to eliminate the initial bias and relax the original configuration. After that, the system temperature is adjusted to the required temperature (300 K and 333 K) by a 2 ns *NPT* simulation, and another 2 ns *NPT* simulation at the corresponding temperature is carried out to balance the configuration. When the total energy does not change over time, the systems are considered to have reached the equilibrium state. The data are collected during the last 10 ns with an interval of 2 ps.

2.4. Diffusion coefficient

The self-diffusion coefficient (D_i) of the SPE is calculated through mean squared diffusion (MSD):

$$D_i = \lim_{t\to\infty} \frac{[R_i(t) - R_i(0)]^2}{6t} \quad (7)$$

where $R_i(t)$ is the vector position. The self-diffusion coefficient is proportional to the MSD.

In MD simulations, the conductivity (σ) can be calculated by the Nernst–Einstein relation:

$$\sigma = \sum q_i n_i \mu_i = \sum \frac{n_i q_i^2 D_i}{k_B T} \quad (8)$$

where n_i is the ion concentration, q_i is the charge of the ionic species, μ_i is the ion mobility, D_i is the equivalent ion diffusivity, T is the temperature, and k_B is the Boltzmann constant.

2.5. Radial distribution function (RDF)

The radial distribution function is the probability of finding particle B at radius r from particle A. The RDF is an important function to describe the structure of molecular systems, which can be expressed as:

$$g_{A-B}(r) = \left(\frac{n_B}{4\pi r^2 dr}\right) \Big/ \left(\frac{N_B}{V}\right) \quad (9)$$

where n_B is the number of B particles in the dr-thick spherical shell at radius r from A particles, $4\pi r^2 dr$ is the volume of the shell, N_B is the total number of B particles in the simulation system, and V is the volume of the simulation system.

2.6. Glass transition temperatures

The glass transition temperature (T_g) refers to the temperature corresponding to the transition from the glass state to the high elastic state. In terms of molecular structure, T_g is a relaxation phenomenon in which the amorphous part of the polymer changes from the frozen state to the thawed state. To compare the T_g, we used a quasi-equilibrium release method to cool the SPE from a high temperature, which is 50 K higher than the T_g predicted by Flory-Fox.[43] Specifically, the temperature is reduced with a step of 10 K.[44] Then, a 1 ns *NPT* simulation is carried out to balance the system and another 1 ns *NPT* simulation is carried out to obtain the system density, which is equivalent to a 0.5 × 10^{10} K s^{-1} cooling rate. The temperature where the slope of dρ/dK has the largest deviation is defined as T_g.

3. Results and discussion

3.1. Model validation

The conductivities simulated by MD simulations at different temperatures are compared with previous experimental results to validate the molecular models used in this work. As shown in Fig. 2(a), the simulated conductivity increases as the temperature increases, which is consistent with the experimental results.[45] As the temperature increases, the polymer electrolyte easily expands to create a larger free space, resulting in an increase in conductivity. Moreover, the linear relationship between log σ and T^{-1} shown in Fig. 2(a) suggests that the conductivity follows the Arrhenius theory and Vogel–Tamman–Fulcher (VTF) equation. The Li$^+$ and TFSI$^-$ diffusion coefficients of PEO-LiTFSI electrolytes with different PEO molecular weights at 363 K are also computed, as shown in Fig. 2(b), which agrees well with the previous works.[46] The samples in MD simulations cannot be as

Open Access Article. Published on 15 March 2022. Downloaded on 2/16/2026 9:13:57 PM.
This article is licensed under a Creative Commons Attribution 3.0 Unported Licence.

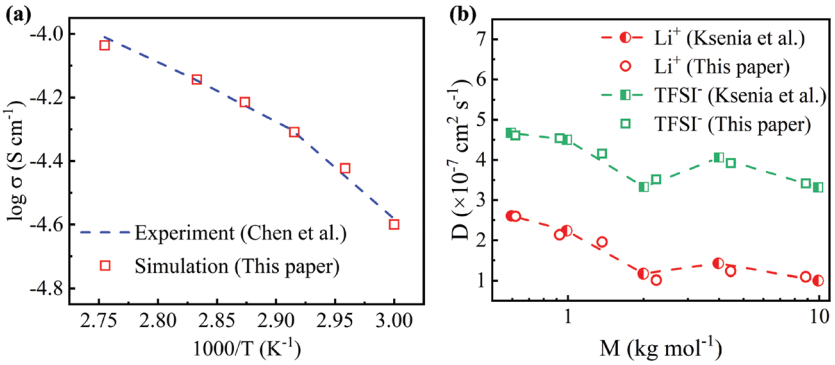

Fig. 2 (a) Simulated conductivity and (b) diffusion coefficients of PEO-LiTFSI electrolytes and comparison with the previous experimental and simulated results.[45,46]

large as the ones in experiments, which leads to the differences between the simulated and experimental results.

3.2. Transport properties

Due to the different numbers of Al_2O_3 nanoparticles, the concentrations of Al_2O_3 in the SC system are 1.3, 4.8, 9.2, 13.2, 15.9, and 18.5 wt%, while those in the LC system are 1.3, 4.5, 8.1, 11.9, 15.0, and 18.3 wt%.[25] The MSD as shown in Fig. S1 and S2 (ESI†) is obtained to compute the diffusivity following eqn (7). The diffusivities of Li^+ and $TFSI^-$ in the SC system and LC system are computed and shown in Fig. 3 and Fig. S3 (ESI†), respectively.

Fig. 3 shows that the addition of Al_2O_3 nanoparticles has a significant impact on the diffusivities of Li^+ and $TFSI^-$. Both the diffusivities of Li^+ and $TFSI^-$ increase first and then decrease with increasing Al_2O_3 mass fraction. The diffusivities of Li^+ and $TFSI^-$ in the SPE filled with 9.2 wt% and 8.1 wt% Al_2O_3 are highest for the SC and LC systems, respectively, which means that the Al_2O_3 nanoparticles enhance Li^+ and $TFSI^-$ transport. In addition, high temperatures make ions move faster, so both the diffusivities of Li^+ and $TFSI^-$ at 333 K are higher than those at 300 K. Generally, $TFSI^-$ shows a higher diffusivity, which is consistent with the simulation results.[33]

Fig. 4 shows the conductivity of PEO-LiTFSI with different mass fractions of Al_2O_3 nanoparticles. As shown in Fig. 4, the

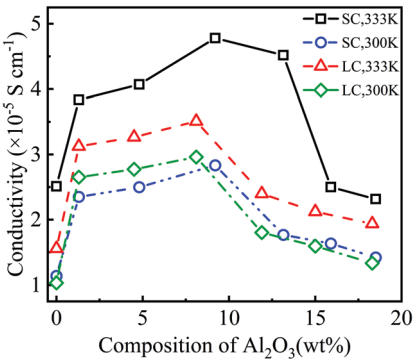

Fig. 4 Conductivities of SPE with different mass fractions of Al_2O_3.

conductivity first increases and then decreases with increasing Al_2O_3 mass fraction, showing the highest values at Al_2O_3 mass fractions of 9.2 wt% and 8.2 wt% for the SC and LC systems, respectively. Moreover, the conductivity at the Al_2O_3 mass fraction of 9.2 wt% is increased by 192.25% and 248.94% at 333 K and 300 K for the SC system, respectively, compared to that without Al_2O_3. The conductivity at the Al_2O_3 mass fraction of 8.2 wt% is increased by 225.2% and 285% at 333 K and 300 K for the LC system, respectively, compared to that without Al_2O_3. B. Scrosati *et al.*[31] found that the addition of TiO_2 can improve

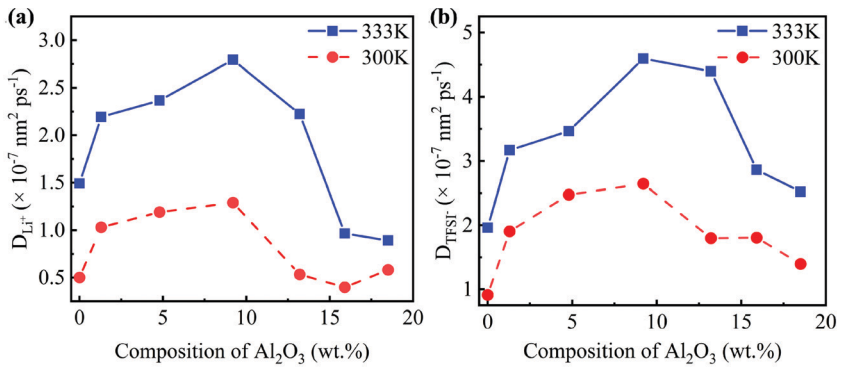

Fig. 3 Diffusivities of (a) Li^+ and (b) $TFSI^-$ at different temperatures in the SC system.

© 2022 The Author(s). Published by the Royal Society of Chemistry

Open Access Article. Published on 15 March 2022. Downloaded on 2/16/2026 9:13:57 PM.
This article is licensed under a Creative Commons Attribution 3.0 Unported Licence.

the conductivity of PEO-$LiCF_3SO_3$ electrolyte to $\sim 10^{-5}$ S cm^{-1} at 333 K, while Y. Matsuo *et al.*[24] found that the SiO_2 fillers can improve the conductivity to 4.4×10^{-5} S cm^{-1} at 303 K, both of which are similar to our results. At a lower Al_2O_3 mass fraction, the increasing Al_2O_3 nanoparticles lead to the interconnection of highly conductive areas near the Al_2O_3, thereby improving the conductivity. However, at a higher Al_2O_3 mass fraction, the Al_2O_3 nanoparticles that are too close to each other increase the polymerization degree of PEO chains, thereby decreasing the conductivity.

Additionally, the conductivity at 333 K is higher than that at 300 K, as shown in Fig. 4, which is consistent with the experimental data.[25] The enhancement effect of Al_2O_3 on the conductivity is stronger at lower temperatures. Furthermore, the conductivity is lower for the SPE with longer PEO chains due to their higher polymerization degree. The addition of Al_2O_3 nanoparticles more highly reduces the polymerization degree of longer PEO chains. Consequently, the increase in the conductivity of the SPE with longer PEO chains is more obvious when adding Al_2O_3, as shown in Fig. 4.

3.3. Structural properties

The RDFs are calculated to explore the structural characteristics of SPEs with Al_2O_3 nanoparticles. Fig. 5 shows the RDFs between Li^+ and O atoms in PEO (Li^+–O (PEO)) and between Li^+ and O atoms in $TFSI^-$ (Li^+–O (TFSI)) in the SC system. As shown in Fig. 5(a and c), the RDFs of Li^+–O (PEO) show a sharp peak at the same position of 1.95 Å, which is consistent with previous studies.[13,33] When the mass fraction of Al_2O_3 is 9.2 wt%, the peak height of the RDF of Li^+–O (PEO) is highest, while that of the RDF of Li^+–O (TFSI) is lowest. This means that the lithium ions are closer to the PEO chains and farther away from $TFSI^-$ when adding Al_2O_3, and thus, the transport of Li^+ along the PEO chains is enhanced, thereby resulting in an increase in conductivity, as shown in Fig. 4. The coordination numbers (CNs) of Li^+–O (PEO) and Li^+–O (TFSI) are calculated and shown in Fig. S4 (ESI†). The CN of Li^+–O (PEO) increases up to approximately 3, and the CN of Li^+–O (TFSI) drops to 2.5 when the mass fraction of Al_2O_3 is 9.2 wt%, which also illustrates that the combination of Li and PEO chains is strengthened by the addition of Al_2O_3. The CN of Li^+–O (PEO) slightly increases, meaning that the addition of Al_2O_3 slightly enhances the Li^+ transport along the PEO chains, which is agreeable with the previous works.[35] However, the CN of Li^+–O (TFSI) was found to greatly decrease when the Al_2O_3 amount increases, which means that more Li^+ can freely migrate at the interface, thereby significantly increasing the conductivity. However, excess Al_2O_3 nanoparticles will aggregate together and suppress the combination of Li^+ and PEO chains, reducing the conductivity, as shown in Fig. 4. In addition, the peak height of the RDF of Li^+–O (PEO) is higher at higher temperatures, meaning that more Li^+ combines with the PEO chains at higher temperatures; thus, the conductivity is higher, as shown in Fig. 4. Furthermore, the larger increase in the peak height of the RDF of Li^+–O (PEO) also explains the larger increase in the conductivity of SPE at 300 K than that at 333 K.

The RDFs and the CNs of the LC system are shown in Fig. 6 and Fig. S5 (ESI†), respectively. The peak height of the RDF of Li^+–O (PEO) is highest, while that of the RDF of Li^+–O (TFSI) is lowest at the Al_2O_3 mass fraction of 8.2 wt%; thus, the

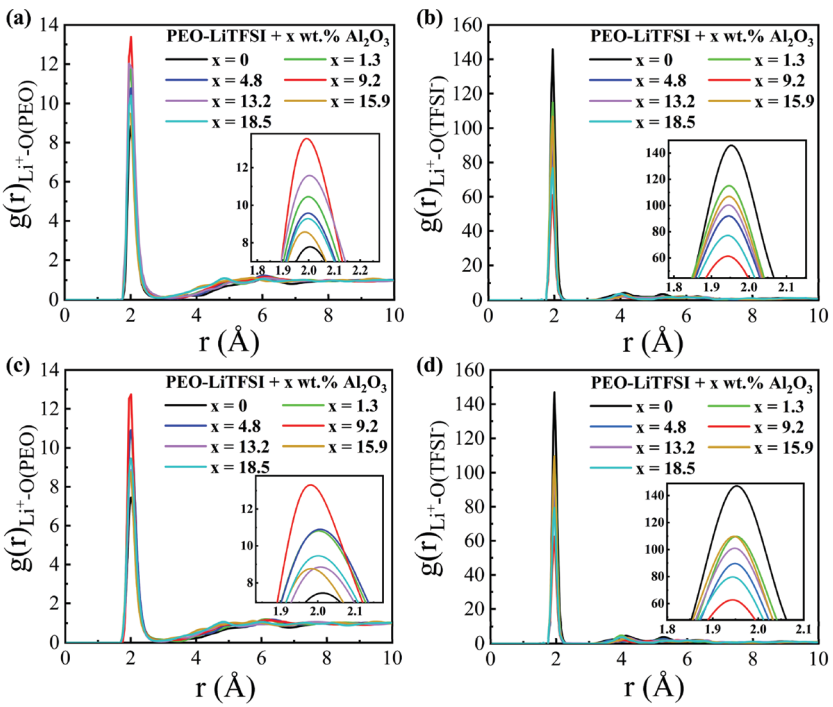

Fig. 5 RDFs of (a) Li^+–O(PEO) at 333 K, (b) Li^+–O(TFSI) at 333 K, (c) Li^+–O(PEO) at 300 K, and (d) Li^+–O(TFSI) at 300 K in the SC systems. PEO-LiTFSI + *x* wt% Al_2O_3 represents PEO-LiTFSI with *x* wt% Al_2O_3. *x* is the mass fraction of Al_2O_3. The insets show an enlargement of the first coordination shell.

Open Access Article. Published on 15 March 2022. Downloaded on 2/16/2026 9:13:57 PM.
This article is licensed under a Creative Commons Attribution 3.0 Unported Licence.

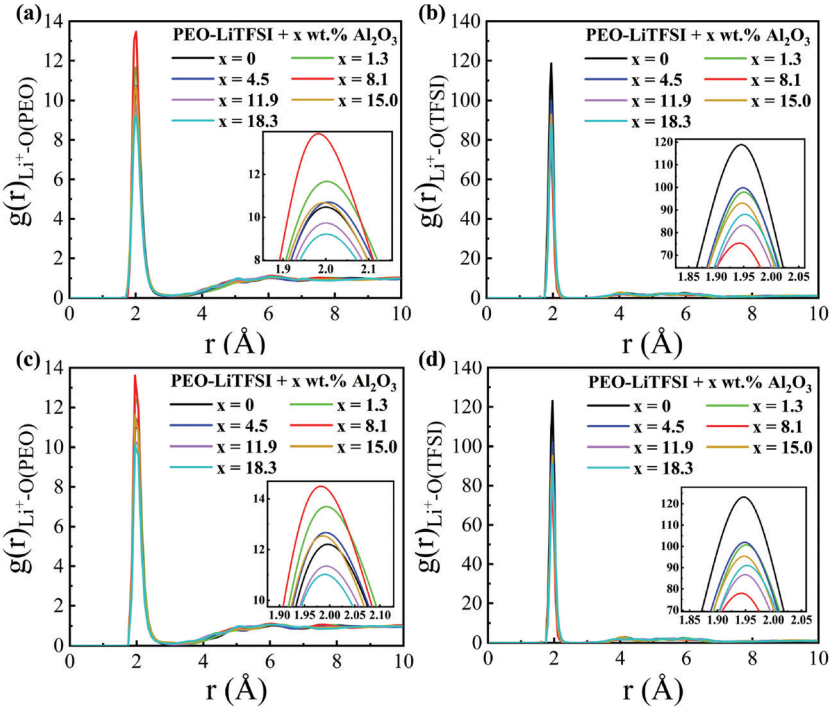

Fig. 6 RDFs for (a) Li^+–O(PEO) at 333 K, (b) Li^+–O(TFSI) at 333 K, (c) Li^+–O(PEO) at 300 K, and (d) Li^+–O(TFSI) at 300 K in the LC systems. The insets show the enlargement of the first coordination shell.

conductivity is highest, as shown in Fig. 4. Different from the SC system, the peak value of the RDF of Li^+–O(PEO) at a higher Al_2O_3 mass fraction is even lower than that without Al_2O_3. When the concentration of Al_2O_3 is too large, the suppression effect of Al_2O_3 on the combination of Li^+ and PEO chains is more obvious in the LC system than in the SC system.

3.4. Glass transition temperatures (T_g)

The densities of the SPE with 0 and 9.2 wt% Al_2O_3 for the SC system and the SPE with 0 and 8.3 wt% Al_2O_3 for the LC system at different temperatures are calculated. As shown in Fig. 7, the T_g drops from 211.18 K to 207.65 K in the SC system, while it drops from 211.56 K to 199.14 K in the LC system. The results show that the addition of Al_2O_3 reduces the T_g of SPE due to the increase in the amorphous region of PEO. Furthermore, the increasing amorphous region will make the PEO chains more flexible, thereby resulting in Li^+ more easily migrating in the amorphous region. Furthermore, the T_g for the LC system is lower than that of the SC system after adding Al_2O_3, which is the main reason that the addition of Al_2O_3 has a stronger enhancement effect on the conductivity of the LC system.

3.5. Transport mechanism

Fig. 8 shows the structural changes of PEO chains and the Li^+ transport paths after adding Al_2O_3 nanoparticles. Generally, the PEO chains have higher crystallinity, and thus, lithium ions have difficulty combining with and moving along the PEO chains, as shown in the left image in Fig. 8. Therefore, the conductivity of SPE is low, significantly limiting its commercial applications. The addition of Al_2O_3 nanoparticles alters the structure of the PEO chains. Specifically, the crystallinity of the PEO chains decreases, and their degree of order increases, as

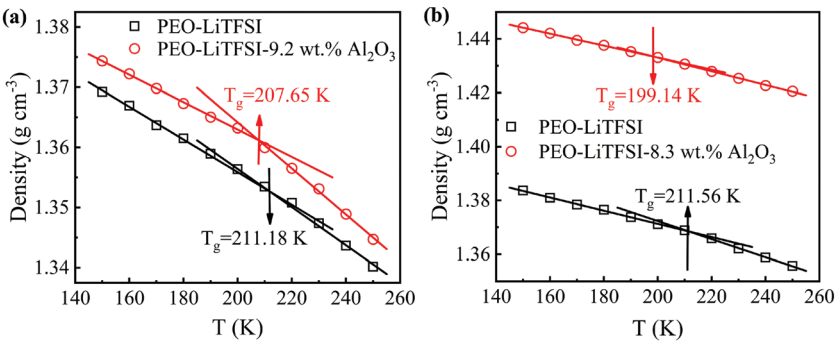

Fig. 7 Densities of the SPE at different temperatures for (a) the SC system and (b) the LC system.

© 2022 The Author(s). Published by the Royal Society of Chemistry

Open Access Article. Published on 15 March 2022. Downloaded on 2/16/2026 9:13:57 PM.
This article is licensed under a Creative Commons Attribution 3.0 Unported Licence.

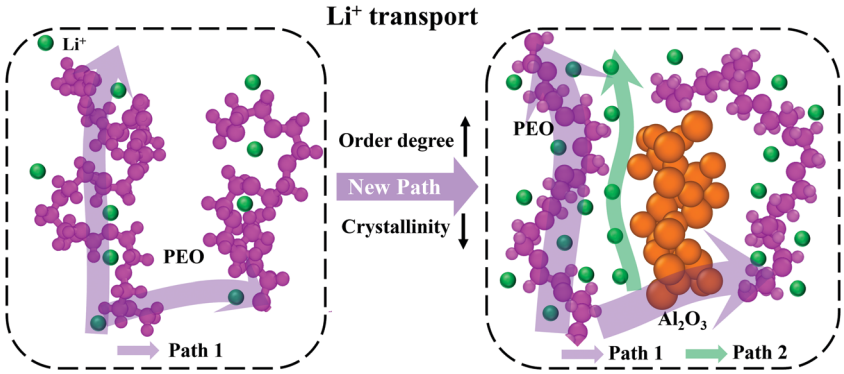

Fig. 8 Structural changes of the PEO chains and Li^+ transport paths after adding Al_2O_3 nanoparticles.

shown in the right image in Fig. 8. Meanwhile, more lithium ions can combine with the PEO chains and move freely along the PEO chains (Path 1). It is noteworthy that the main transport path of Li^+ is along the PEO chains.[13] Moreover, the simulation results show that a number of lithium ions transport at the interface between Al_2O_3 and the PEO chains, indicating that the addition of Al_2O_3 provides an additional path for Li^+ transport (Path 2). Therefore, the conductivity of SPE is significantly increased by the Al_2O_3 nanoparticles. However, at high mass fractions, excess Al_2O_3 nanoparticles will aggregate together and block the transport of Li^+.

4. Conclusions

The structure and transport properties of SPEs filled with Al_2O_3 nanoparticles are explored by all-atom MD simulations. The MD model is verified by comparing the conductivity with the experimental results. The effects of Al_2O_3 nanoparticles on the conductivity of SPEs with different PEO chain lengths at different temperatures are studied. The simulation results show that the conductivity is increased by 192.25% and 248.94% at 333 and 300 K, respectively, for the shorter PEO chains and increased by 225.2% and 285% at 333 and 300 K, respectively, for the longer PEO chains. This suggests that the effects of Al_2O_3 nanoparticles on the conductivity are more significant for longer PEO chains at lower temperatures. The increase in conductivity is attributed to the structural changes that occur in the SPE upon addition of Al_2O_3 nanoparticles. The addition of Al_2O_3 makes Li^+ more easily combine with PEO chains and reduces combination with $TFSI^-$, which is beneficial to Li^+ transport along the PEO chains. Moreover, the crystallinity is studied by computing the T_g of SPE. The results show that the crystallinity of the PEO chains decreases and the degree of order increases when adding Al_2O_3 nanoparticles, which also benefits Li^+ transport along the PEO chains. On the other hand, the addition of Al_2O_3 provides an additional Li^+ transport path, which is the interface between the Al_2O_3 and PEO chains. Therefore, the conductivity of the PEO chains is increased significantly by Al_2O_3 nanoparticles. These findings are highly valuable for insights into the structure and transport characteristics of SPEs and the fundamental understanding of Al_2O_3's effects in SPEs.

Conflicts of interest

The authors declare that they have no known competing financial interests or personal relationships that could have appeared to influence the work reported in this paper.

Acknowledgements

This research is supported by the National Natural Science Foundation of China (Grant No. 51921004), and the Natural Science Foundation of Tianjin (China) for Distinguished Young Scholars (Grant No. 18JCJQJC46700).

References

1 K. Jiao, J. Xuan, Q. Du, Z. Bao, B. Xie, B. Wang, Y. Zhao, L. Fan, H. Wang, Z. Hou, S. Huo, N. P. Brandon, Y. Yin and M. D. Guiver, *Nature*, 2021, **595**, 361–369.
2 D. Jin and K. Jiao, *Joule*, 2020, **4**, 1634–1636.
3 A. Perner and J. Vetter, in *Advances in Battery Technologies for Electric Vehicles*, ed. B. Scrosati, J. Garche and W. Tillmetz, Woodhead Publishing, 2015, 173–190.
4 D. Cao, X. Sun, Q. Li, A. Natan, P. Xiang and H. Zhu, *Matter*, 2020, **3**, 57–94.
5 Y. Lin, J. Li, K. Liu, Y. Liu, J. Liu and X. Wang, *Green Chem.*, 2016, **18**, 3796–3803.
6 M. Forsyth, L. Porcarelli, X. Wang, N. Goujon and D. Mecerreyes, *Acc. Chem. Res.*, 2019, **52**, 686–694.
7 L.-Z. Fan, X.-L. Wang and F. Long, *J. Power Sources*, 2009, **189**, 775–778.
8 G. Wang, X. Zhu, A. Rashid, Z. Hu, P. Sun, Q. Zhang and L. Zhang, *J. Mater. Chem. A*, 2020, **8**, 13351–13363.
9 C. H. Wang, Y. F. Yang, X. J. Liu, H. Zhong, H. Xu, Z. B. Xu, H. X. Shao and F. Ding, *ACS Appl. Mater. Interfaces*, 2017, **9**, 13694–13702.
10 M. Wetjen, M. A. Navarra, S. Panero, S. Passerini, B. Scrosati and J. Hassoun, *ChemSusChem*, 2013, **6**, 1037–1043.
11 E. Quartarone and P. Mustarelli, *Chem. Soc. Rev.*, 2011, **40**, 2525–2540.

Open Access Article. Published on 15 March 2022. Downloaded on 2/16/2026 9:13:57 PM.
This article is licensed under a Creative Commons Attribution 3.0 Unported Licence.

12 V. R. Sunitha and S. Radhakrishnan, Field enhanced Li ion conduction in nanoferroelectric modified polymer electrolyte systems, *Ionics*, 2014, **21**, 949–954.
13 D. J. Brooks, B. V. Merinov, W. A. Goddard, B. Kozinsky and J. Mailoa, *Macromolecules*, 2018, **51**, 8987–8995.
14 D. Devaux, R. Bouchet, D. Glé and R. Denoyel, *Solid State Ionics*, 2012, **227**, 119–127.
15 O. Borodin and G. D. Smith, *Macromolecules*, 2006, **39**, 1620–1629.
16 H.-S. Liu, K.-Y. Chen, C.-E. Fang and C.-C. Chiu, *Electrochim. Acta*, 2021, **375**, 137915.
17 J. Yu, M. Lee, Y. Kim, H.-K. Lim, J. Chae, G. S. Hwang and S. Lee, *J. Power Sources*, 2021, **505**, 229917.
18 Q. Liu, B. Peng, M. Shen, B. Hu and Q. Chen, *Solid State Ionics*, 2014, **255**, 74–79.
19 O. Borodin and G. D. Smith, *J. Solution Chem.*, 2007, **36**, 803–813.
20 C. Deng, M. A. Webb, P. Bennington, D. Sharon, P. F. Nealey, S. N. Patel and J. J. de Pablo, *Macromolecules*, 2021, **54**, 2266–2276.
21 S. Li, S. Q. Zhang, L. Shen, Q. Liu, J. B. Ma, W. Lv, Y. B. He and Q. H. Yang, *Adv. Sci.*, 2020, **7**, 1903088.
22 Y. J. Lim, H. W. Kim, S. S. Lee, H. J. Kim, J. K. Kim, Y. G. Jung and Y. Kim, *ChemPlusChem*, 2015, **80**, 1100–1103.
23 S. Ketabi and K. Lian, *Electrochim. Acta*, 2013, **103**, 174–178.
24 Y. Matsuo and J. Kuwano, *Solid State Ionics*, 1995, **79**, 295–299.
25 M. R. Johan, O. H. Shy, S. Ibrahim, S. M. Mohd Yassin and T. Y. Hui, *Solid State Ionics*, 2011, **196**, 41–47.
26 B. W. Zewde, S. Admassie, J. Zimmermann, C. S. Isfort, B. Scrosati and J. Hassoun, *ChemSusChem*, 2013, **6**, 1400–1405.
27 H.-M. Xiong, Z.-D. Wang, D.-P. Xie, L. Cheng and Y.-Y. Xia, *J. Mater. Chem.*, 2006, **16**, 1345–1349.
28 Y. Zhang, X. Wang, W. Feng, Y. Zhen, P. Zhao, Z. Cai and L. Li, *Ionics*, 2018, **25**, 1471–1480.
29 S. R. Yeandel, B. J. Chapman, P. R. Slater and P. Goddard, *J. Phys. Chem. C*, 2018, **122**, 27811–27819.
30 Y. Zheng, Y. Yao, J. Ou, M. Li, D. Luo, H. Dou, Z. Li, K. Amine, A. Yu and Z. Chen, *Chem. Soc. Rev.*, 2020, **49**, 8790–8839.
31 B. W. Zewde, G. A. Elia, S. Admassie, J. Zimmermann, M. Hagemann, C. S. Isfort, B. Scrosati and J. Hassoun, *Solid State Ionics*, 2014, **268**, 174–178.
32 N. Boaretto, I. Garbayo, S. Valiyaveettil-SobhanRaj, A. Quintela, C. M. Li, M. Casas-Cabanas and F. Aguesse, *J. Power Sources*, 2021, **502**, 229919.
33 M. Ebadi, L. T. Costa, C. M. Araujo and D. Brandell, *Electrochim. Acta*, 2017, **234**, 43–51.
34 V. Ponce, D. E. Galvez-Aranda and J. M. Seminario, *Phys. Chem. Chem. Phys.*, 2021, **23**, 597–606.
35 Q. Li and H. Ardebili, *Solid State Ionics*, 2014, **268**, 156–161.
36 W. L. Jorgensen, D. S. Maxwell and J. Tirado-Rives, *J. Am. Chem. Soc.*, 1996, **118**, 11225–11236.
37 S. Plimpton, *J. Comput. Phys.*, 1995, **117**, 1–19.
38 F. Croce, S. Sacchetti and B. Scrosati, *J. Power Sources*, 2006, **162**, 685–689.
39 K. Persson, *Materials Data on Al_2O_3 (SG:167) by Materials Project, 2014.*
40 R. Khodabandeh, F. Mohammadpour, A. R. Zolghadr and A. Klein, *New J. Chem.*, 2020, **44**, 16602–16612.
41 Q. Li, H. Y. Sun, Y. Takeda, N. Imanishi, J. Yang and O. Yamamoto, *J. Power Sources*, 2001, **94**, 201–205.
42 M. A. K. L. Dissanayake, P. A. R. D. Jayathilaka, R. S. P. Bokalawala, I. Albinsson and B. E. Mellander, *J. Power Sources*, 2003, **119**, 409–414.
43 T. P. Lodge and T. C. B. McLeish, *Macromolecules*, 2000, **33**, 5278–5284.
44 S. Mogurampelly and V. Ganesan, *Macromolecules*, 2018, **51**, 9471–9483.
45 H. Chen, D. Adekoya, L. Hencz, J. Ma, S. Chen, C. Yan, H. Zhao, G. Cui and S. Zhang, *Adv. Energy Mater.*, 2020, **10**, 2000049.
46 K. Timachova, H. Watanabe and N. P. Balsara, *Macromolecules*, 2015, **48**, 7882–7888.

© 2022 The Author(s). Published by the Royal Society of Chemistry